LA-5502-MS
INFORMAL REPORT

Heat Transfer and Thermal Treatment Processes in Subterrene-Produced Glass Hole Linings

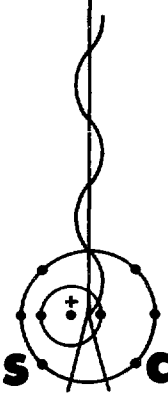

los alamos
scientific laboratory
of the University of California
LOS ALAMOS, NEW MEXICO 87544

UNITED STATES
ATOMIC ENERGY COMMISSION
CONTRACT W-7405-ENG. 36

In the interest of prompt distribution, this LAMS report was not edited by the Technical Information staff.

Printed in the United States of America. Available from
National Technical Information Service
U. S. Department of Commerce
5285 Port Royal Road
Springfield, Virginia 22151
Price: Printed Copy $4.00; Microfiche $1.45

LA-5502-MS
Informal Report
UC-38
ISSUED: February 1974

los alamos
scientific laboratory
of the University of California
LOS ALAMOS, NEW MEXICO 87544

Heat Transfer and Thermal Treatment Processes in Subterrene-Produced Glass Hole Linings

by

A. E. Stanton*

*LASL Summer Graduate Student, 1973. Present address: Stanford University, Stanford, California 94305.

Work supported in part by a grant from National Science Foundation, Research Applied to National Needs (RANN).

HEAT TRANSFER AND THERMAL TREATMENT PROCESSES IN SUBTERRENE-PRODUCED GLASS HOLE LININGS

by

A. C. Stanton

ABSTRACT

Glass-forming and thermal treatment processes for the glass liners of bore holes produced by Subterrene rock-melting penetrators are considered. Analytical and numerical calculations of the radial temperature distributions and glass cooling rates are reported for the glass-like liners created by laboratory penetrators operating in local Los Alamos tuff and basalt. The temperature calculations are compared with experimental data. The cooling rate at the inside surface of the glass liner is strongly influenced by the penetrator afterbody and stem design. To minimize residual stresses in the cooled glass, a qualitative correlation is found between this cooling rate and the thermal properties of the parent rock. The magnitude of residual strains and stresses in glass produced by laboratory penetrators is estimated.

I. INTRODUCTION

The development and testing of small rock-melting penetrators at the Los Alamos Scientific Laboratory has opened the way for important advances in the three major elements of the drilling or tunneling process:

- Formation of the hole or tunnel,
- Support of the tunnel or bore-hole wall, and
- Handling and removal of the debris.

The liquid form of the rock melt accounts for the new contributions to solutions in these three areas. Prototype penetrators that consolidate the melted rock into a dense glass lining have been developed for use in low-density or unconsolidated formations.[1] These devices, which have solid cross sections, are called melting-consolidating penetrators. Other designs, called universal extruding penetrators, allow for the extrusion of rock melt through a central extrusion hole.[2] The melt is chilled into a variety of forms, including glass rods, glass pellets, and rock wool, and is transported up the stem by the coolant flow; a glass lining on the hole can be produced simultaneously. Thus, the universal extruding penetrator has the capability of penetrating dense, hard rock as well as loose or low-density materials. Schematics of the consolidating and extruding penetrators are shown in Figs. 1 and 2.

The glass lining produced by either type of penetrator can be used to case and seal the bore hole. The lining also provides structural support for the hole, which is a particularly important advantage in unconsolidated materials such as alluvium. The improvement or "optimization" of the glass structure is therefore of particular interest. Of special importance is the method by which the rock melt is cooled to form the glass. Various thermal treatments are used in the glass industry to produce desirable characteristics and properties in commercial glasses. This report considers the temperature history and temperature distributions in the glass liner produced by Subterrene rock-melting penetrators and relates these thermal effects to the glass-forming and glass-treatment processes. Temperature calculations are reported for 50- and 75-mm-diam consolidating penetrators in tuff. The results for the 75-mm-diam penetrator also include calculations based on basalt rock properties.

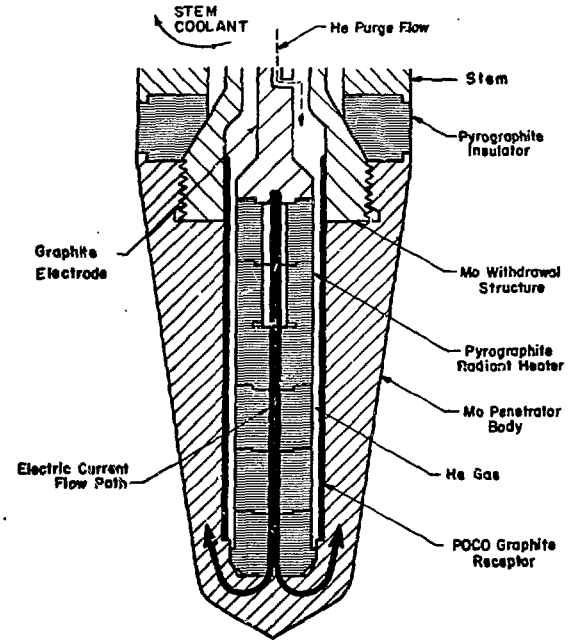

Fig. 1. Melting-consolidating penetrator.

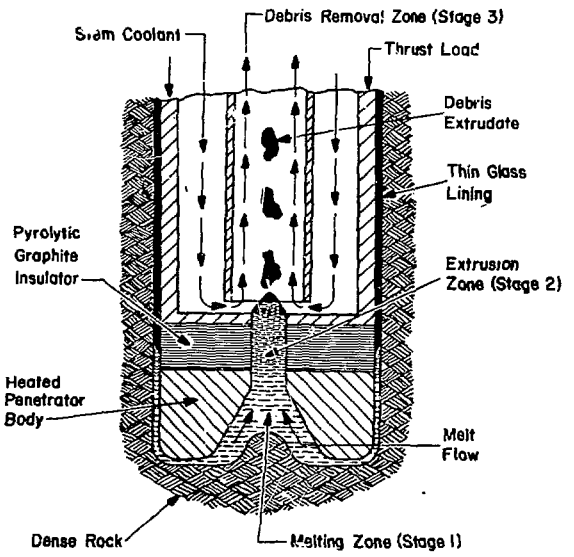

Fig. 2. Universal extruding penetrator.

II. GLASS-FORMING AND THERMAL TREATMENT PROCESSES

A. Glass-Forming With Subterrene Penetrators

Most rock melts consist largely of molten oxide or silicate systems which tend to supercool and to form a glass.[3] Properties of rock glass vary both with the chemical composition of the rock and with the temperature history of the glass. The glass produced by current Subterrene penetrator designs is a heterogeneous material, often containing suspended matter due to incomplete melting. Glass-forming and glass thermal treatment with the Subterrene are subject to many considerations that prevail in the manufacture of commercial glasses.

Prototype Subterrene penetrators have included a pyrolytic-graphite insulator between the high-temperature, refractory-metal penetrator and the afterbody (see Figs. 1 and 2). This insulator creates a large axial temperature difference between the penetrator and the afterbody, resulting in rapid chilling of the rock melt to levels below the fusion temperature of the rock or soil. The insulating washer and the molybdenum or graphite afterbody thus constitute a glass "mold" that forms the glass and provides a rapid initial cooling rate. Experience in the glass industry has shown that the glass may stick to the mold if the melt temperature remains too high.[4] The insulator thus prevents the melt from sticking to the penetrator and thereby avoids both the forming of high shear forces in the cooling, highly viscous melt and the associated impedance to forward motion of the penetrator.[1]

The pyrolytic-graphite insulator is followed by the afterbody. This component, which is cooled by either gas or liquid flowing through the inside of the stem to the afterbody, provides a slower cooling rate for the glass. In the 50-mm-diam penetrator systems the molybdenum afterbody and the stem have the same outside diameter as the penetrator. However, skrinkage of the still viscous melt-glass on cooling and the inevitable surface roughness of the afterbody and stem cause a thin separation layer of air to form between the glass and the stem, which has the effect of additionally slowing down the heat transfer between the glass and the stem.

For the 75-mm-diam penetrator, the graphite afterbody is followed by a stem with an outside diameter of 50 mm, leaving an annular space between the stem and the glass lining. Part of the coolant gas is ducted through this annular space. Cooling

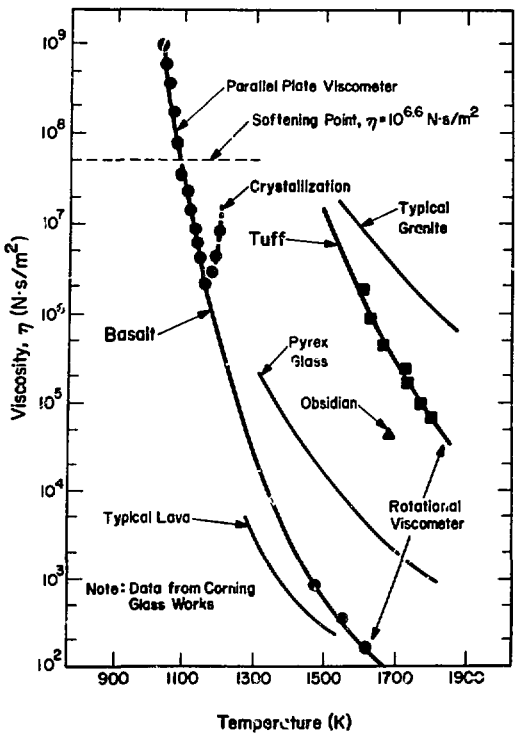

Fig. 3. Experimental viscosity-vs-temperature relationships for Los Alamos tuff and basalt melts.

at the inside surface of the glass is therefore accomplished by convection to the coolant gas and by thermal radiation to the cooler stem.

B. Thermal Treatment of Glass

1. General. A body of glass that is cooled to ambient temperature from the viscous state will have residual internal stresses and strains,[5] which may be sufficiently high to cause undesirable thermal-stress cracking. Because the magnitude of the stresses is primarily determined by the cooling rate through the "transformation range" of temperatures, cooling rates and temperature distributions in Subterrene-produced glass linings must be carefully considered, as is discussed below.

2. Melt Viscosity. Because the viscosity of glass melts is strongly temperature-dependent and because the viscosity-vs-temperature characteristics vary for different rock-melts, important temperature ranges in thermal treatment processes are usually characterized in terms of the melt viscosity, η. Several reference points have been established.[6]

The strain point ($\eta = 10^{13.5}$ N • s/m^2) is the temperature at which internal stresses are significantly reduced in a matter of hours; at the annealing point ($\eta = 10^{12}$ N • s/m^2), internal stresses are reduced to "acceptable commercial limits" within minutes; at the temperature corresponding to the softening point ($\eta = 10^{6.6}$ N • s/m^2), glass melt will rapidly deform under its own weight; and the working point ($\eta = 10^{3}$ N • s/m^2) is the temperature at which the glass melt is soft enough for hot-working. The annealing or transformation range is the range of temperatures between the annealing point and the strain point, and the working range is the temperature range between the working point and the softening point. Experimental determinations of rock-glass viscosity as a function of temperature (shown in Fig. 3) have been made by the Corning Glass Works for samples of Los Alamos basalt and tuff.[7] The tuff melt was significantly more viscous than the basalt melt, a fact that had been qualitatively observed in Subterrene laboratory tests. Table I lists the experimentally determined reference viscosity temperatures for basalt glass. Comparable data for tuff are not available, although the viscosity-vs-temperature curves in Fig. 3 suggest that the corresponding points may be ~ 300 to 400 K higher than the data for basalt.

3. Annealing. The primary purpose of the annealing process is to reduce residual stresses. If the temperature of the glass is held at or slightly above the annealing-point temperature, stresses are relaxed by the viscous deformation of the glass. For nonhomogeneous glasses, a minimum stress level exists beyond which the stresses cannot be reduced.

TABLE I

VISCOSITY REFERENCE-POINT TEMPERATURES FOR LOS ALAMOS BASALT MELT

Reference Point	Viscosity (η), N • s/m^2	Temperature, K
Strain point	$10^{13.5}$	894
Annealing point	10^{12}	924
Softening point	$10^{6.6}$	1085
Working range	$10^{6.6}$ - 10^{3}	1173-1323

When the glass temperature drops below the strain point the deformations become permanent, and when an equilibrium temperature is reached the stresses that were relaxed in the annealing range appear in reverse.[5] Thus, for a section of glass that is hotter inside than on the outside surface, tensile stresses are formed at the surfaces due to greater contraction inside as the glass cools. These stresses are partially relaxed in the annealing range and reappear as compressive stresses when an equilibrium temperature is reached. The net effect is an overall reduction in stress magnitudes.

The stress which the temperature gradient attempts to form at a point is proportional to the difference between the temperature at that point and the average temperature across the section.[5]

$$\sigma = \frac{E\alpha' \Delta T_e}{1 - \nu} \quad . \tag{1}$$

In this expression E is Young's modulus, α' is the coefficient of thermal expansion in the annealing range, ΔT_e is the temperature difference from the average temperature, and ν is Poisson's ratio.

The importance of Eq. (1) is its implication that undesirable thermal stresses in Subterrene glass liners can be minimized by keeping the temperature gradient small as the glass cools through the annealing range. Because temperature differences in the glass are probably proportional to the cooling rate, an ideal "annealing schedule" might be described as follows.

- A rapid initial chilldown from the rock fusion temperature is required to form the glass and to prevent sticking of the melt to Subterrene components.
- As the glass enters the annealing range a slow cooling rate should be used to minimize temperature gradients and to prevent the forming of unacceptably large thermal stresses.
- When the glass temperature drops well below the strain point, faster cooling rates are permissible. Any stresses that appear in this range are temporary because deformations in the glass are already essentially fixed.

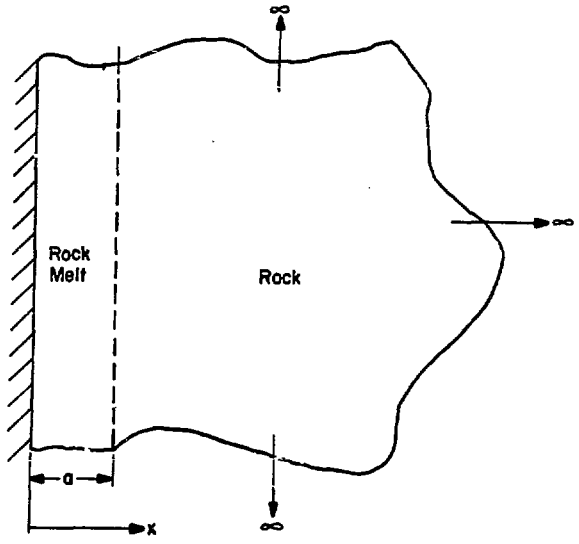

Fig. 4. Geometry for the analytical approximation.

III. THERMAL ANALYSIS MODELS

A. General

Temperature distributions in the glass and surrounding rock were calculated on the basis of several models, including an analytical approximation and computer models. Calculations were made for the 50- and 75-mm-diam, consolidating penetrators in tuff, and the calculations for the 75-mm penetrator were repeated by using properties for basalt melt.

B. Analytical Approximation

The problem was approximated by considering one-dimensional transient heat conduction in a homogeneous isotropic semi-infinite solid in Cartesian coordinates (Fig. 4). The region $0 \le x \le a$ represents the rock melt or glass and $x > a$ is the surrounding unmelted rock. Initial and boundary conditions for the temperature are

$$T(x,0) = \begin{cases} T_o, & 0 \le x \le a \\ T_\infty, & x > a \end{cases} \tag{2}$$

$$\frac{\partial T}{\partial x} = 0 \text{ at } x = 0 \tag{3}$$

$$\lim_{x \to \infty} T(x, t) = T_\infty \quad . \tag{4}$$

The solution[8] to the linear, transient heat-conduction equation which satisfies these conditions is

$$\theta = 1/2 \left(\operatorname{erf} \frac{1-X}{2\sqrt{\tau}} + \operatorname{erf} \frac{1+X}{2\sqrt{\tau}} \right) \qquad (5)$$

where

$\theta = \frac{T - T_\infty}{T_o - T_\infty}$, - a nondimensional temperature;

$X = \frac{x}{a}$, - a nondimensional distance; and

$\tau = \frac{Dt}{a^2}$, - a nondimensional time (Fourier number), where D is thermal diffusivity.

A value of 1450 K was used for T_o. This temperature is in the melting range of the rock. An ambient temperature, T_∞, of 300 K was assumed. The value of thermal diffusivity, D, depends on the rock type, and the glass thickness, a, is dependent on the porosity of the rock. If r_m is the radial distance to the outside of the glass lining and r_p is the inside radius of the lining, then[9], from conservation of mass,

$$\frac{r_m}{r_p} = \sqrt{\frac{1}{P}} \qquad (6)$$

where P is the rock porosity. For tuff this ratio is ~ 1.5. For a 50-mm-diam consolidating penetrator operating in tuff, the glass thickness is ~ 12.5 mm; for a 75-mm-diam consolidator the thickness is ~ 19 mm.

The analytical approximation has several limitations. The formulation neglects conduction in the z-direction; the geometry itself is approximate because the actual situation is one of axially symmetric heat transfer in cylindrical coordinates; the formulation does not allow for variable thermal properties; and the adiabatic boundary condition, Eq. (3), neglects heat transfer to the penetrator stem. However, the solution is still useful in estimating heat-transfer rates to the surrounding rock,* but this effect is exaggerated by the large discontinuity in the assumed initial temperature distribution. The difficulties and limitations of the analytical solution can be mostly overcome by the use of numerical methods.

*The same formulation has been used by J. C. Jaeger to study the cooling of magma intrusions in igneous rock.[10]

C. Computer Models

1. Introduction. A finite-element computer code[11] has been developed at the Los Alamos Scientific Laboratory to solve the energy equation in two dimensions,

$$\nabla \cdot (\underline{\lambda} \cdot \nabla T) + U''' - \rho C \vec{V} \cdot \nabla T = \rho C \frac{\partial T}{\partial t} , \qquad (7)$$

where

$\underline{\lambda}$ = thermal-conductivity tensor,
T = temperature,
U''' = heat generation rate per unit volume,
ρ = material density,
C = specific heat,
$\vec{V}$ = material velocity,
t = time.

A spatially linear temperature relationship is assumed for each triangular element. Flexibility of geometry is preserved by specifying either plane sections or axisymmetric bodies.

The finite-element code was used in two ways to estimate temperature distributions in the glass and surrounding rock.

- Two-dimensional quasi-stationary solutions were obtained which included the material convection term in Eq. (7); and
- One-dimensional transient solutions were calculated for comparison both with the analytical approximation and with the two-dimensional solutions.

2. Two-Dimensional Quasi-Stationary Model. An axisymmetric cylindrical coordinate system was used for the two-dimensional models. The finite-mesh geometry is shown in Fig. 5. The maximum distance along the stem behind the pyrolytic-graphite insulator was 240 mm. The maximum radial distance into the rock for the 50-mm-diam penetrator model was ~ 175 mm, and the corresponding distance for the 75-mm-diam model was ~ 262 mm.

The models included properties for the rock, the rock melt, the molybdenum penetrator and afterbody, and the pyrolytic-graphite insulator. A small

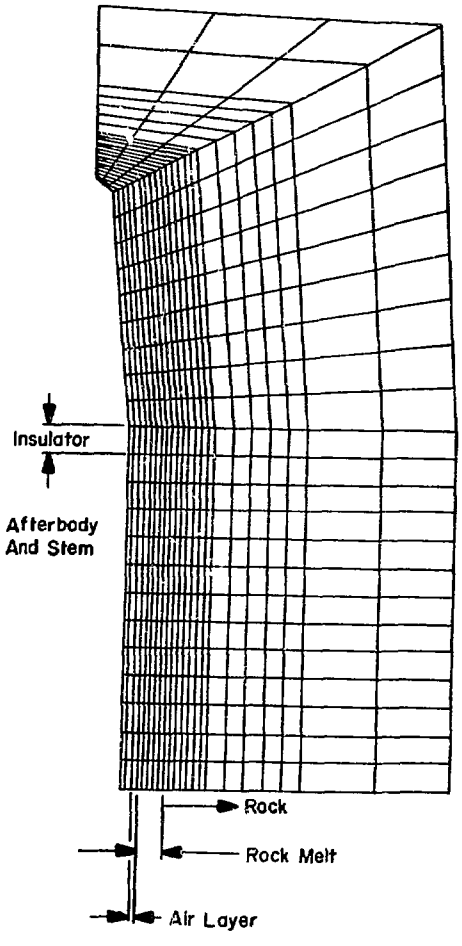

Fig. 5. Finite-element mesh for two-dimensional thermal analysis. (The model shown is for the 50-mm-diam penetrator.)

air gap between the stem and the rock melt was included in the model for the 50-mm-diam penetrator.

Because the problem is steady-state, no initial conditions are required. A penetration rate, $|V_z|$, of 0.15 mm/s was used. A uniform temperature of 1823 K was assumed for the 50-mm-diam penetrator. For the 75-mm-diam case, an assumed penetrator temperature distribution was used to approximate thermocouple data from an experiment conducted in tuff. The boundary along the penetrator axis is adiabatic due to symmetry. Experimental data were used to estimate heat-transfer coefficients to the coolant flow. Flow rates of 4 to 5 g/s are typical, with ~ 40% of the flow returning through the annular space for the case of the 75-mm-diam penetrator. Zero heat

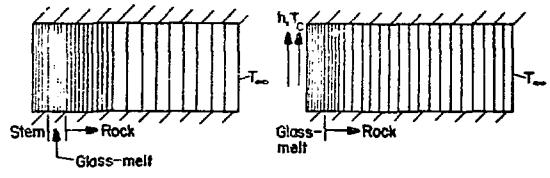

Fig. 6. Geometrical models for one-dimensional transient heat-transfer calculations, (a) 50-mm-diam penetrator, (b) 75-mm-diam penetrator.

flux was assumed through the bottom horizontal plane of the model. This assumption is reasonable, although not strictly true, because the axial temperature gradients are small at large distances from the penetrator and because the thermal conductivity of the rock is low. The remaining boundaries represent rock at comparatively large distances from the penetrator. These boundaries are assumed to be at a constant ambient temperature of 300 K.

For the model of the 75-mm-diam penetrator, thermal radiation from the inside surface of the glass to the stem was approximated by calculating effective heat-transfer coefficients to account for the combined convection-and-radiation boundary condition. A discussion of the approximate radiation boundary condition is contained in the appendix.

3. One-Dimensional Transient Models. The one-dimensional models treated the problem as one of transient radial flow in an infinite annular region without material convection. For this case the differential equation of heat conduction is

$$\rho C \frac{\partial T}{\partial t} = \frac{1}{r} \frac{\partial}{\partial r} \left[r\lambda \frac{\partial T}{\partial r} \right] . \qquad (8)$$

The geometrical models for the finite-element mesh are shown in Fig. 6.

Results from the two-dimensional calculations were used to develop the initial conditions. The calculated temperature distribution along the horizontal plane extending from the aft edge of the pyrolytic-graphite insulator was approximated by piecewise polynomials.

Boundary conditions at the left edge of the regions shown in Fig. 6 were expressed in terms of a heat-transfer coefficient and an assumed bulk

temperature of the coolant flow. Both quantities were estimated on the basis of test data. A temperature of 500 K was used for the coolant. An effective heat-transfer coefficient was used in the 75-mm-diam model to account for thermal radiation to the stem (see appendix).

The right edge of the models was assumed to be at an infinite distance from the penetrator so that the temperature is the ambient temperature, 300 K. For both penetrator models a maximum radial distance of 300 mm into the rock was assumed.

In addition to the solutions satisfying the conditions above, the one-dimensional models were used to investigate variations of both the problem and the boundary conditions. Calculations were made where heat transfer from the glass was limited either to conduction into the rock or to heat loss into the stem and the coolant. The effect of removing the radiation boundary conditions was also investigated.

D. Rock and Rock-Glass Properties

Physical and thermal properties of the rocks and rock glasses that were used in the analyses are shown in Table II. Two values for the thermal conductivity of tuff were used. The lower value, 0.25 W/m·K, has been measured on samples of Los Alamos tuff, whereas 0.75 W/m·K is a typical value based on literature data.[12] The thermal conductivity for the rock glasses is an "effective" conductivity which includes contributions due to thermal radiation.[9]

IV. RESULTS OF TEMPERATURE CALCULATIONS

A. Temperature-vs-Time Results

1. General. The one-dimensional transient calculations were carried out through a total cooling time of 7200 s, which represents the time elapsed from final contact with the pyrolytic-graphite insulator and is equal to a distance of 1.08 m for a penetration rate of 0.15 mm/s. For the two-dimensional analyses based on a constant penetration rate of 0.15 mm/s, the maximum axial distance from the penetrator is equivalent to a cooling time of 1600 s.

Figures 7 through 9 show the calculated cooling curves for a fixed point on the surface of the inside diameter of the glass lining. A room-temperature thermal conductivity for tuff of 0.25 W/m·K was used. Results for the 75-mm-diam penetrator include the approximate radiation boundary condition.

As illustrated by the cooling curves, heat transfer in the radial direction is the dominant effect. For all three cases the one- and two-dimensional computer results agree to within 1 or 2%. This fact suggests that the two-dimensional results for longer cooling times (or, equivalently, greater axial distances) can be estimated by the one-dimensional computer analysis. Consequently, large savings on computational time and storage needs are possible because a two-dimensional analysis would require many finite elements.

Because of the simplifications involved, the analytical approximation cannot be expected to accurately represent the physical problem, although good agreement with the computer results can be noted for the 75-mm-diam penetrator in tuff. The much larger disparity between the analytical and numerical results for the 50-mm-diam penetrator is probably caused by geometric considerations and by the discontinuity in the initial conditions. The error in approximating the cylindrical geometry by a rectangular slab increases as radial distances

TABLE II

PROPERTIES OF ROCK AND ROCK-GLASS

Material	Density (ρ), Mg/m^3	Specific Heat (C), kJ/kg·K	Thermal Conductivity (λ), W/m·K, at 300 K	Thermal Diffusivity (D), m^2/s	Melting Point (Tm), K
Tuff	1.4	1.0	0.25, 0.75	1.79×10^{-7}, 5.36×10^{-7}	1420
Tuff-glass	2.5	1.38	5.46 (1500 K)	1.58×10^{-6}	--
Basalt	2.7	1.0	1.5	5.56×10^{-7}	1420
Basalt-glass	2.75	1.38	5.46 (1500 K)	1.44×10^{-6}	--

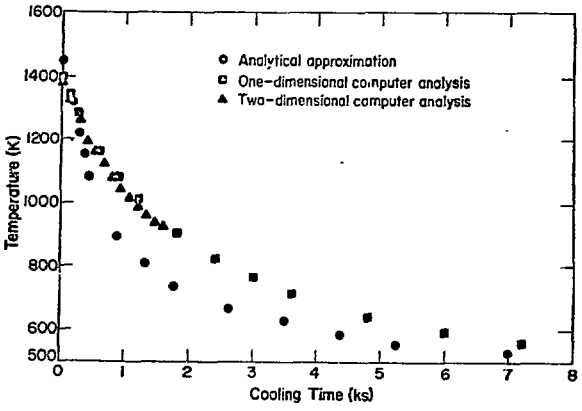

Fig. 7. Glass-liner temperature at the inside diameter; 50-mm penetrator in tuff.

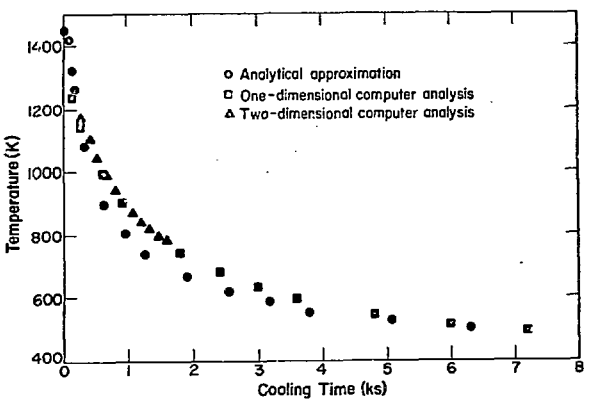

Fig. 9. Glass-liner temperature at the inside diameter; 75-mm penetrator in basalt.

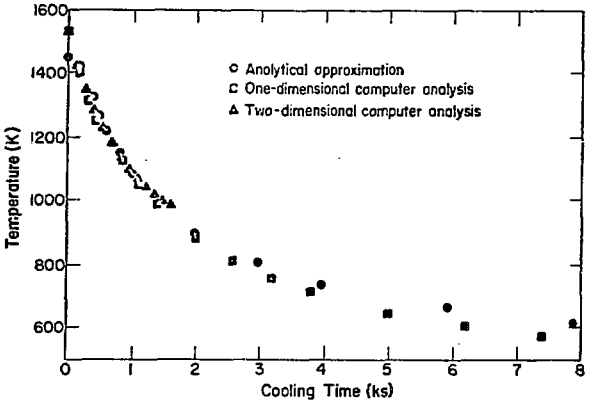

Fig. 8. Glass-liner temperature at the inside diameter; 75-mm penetrator in tuff.

become smaller. Also, the effect of the discontinuity in the initial conditions becomes more important for thinner glass sections. The influence of the discontinuity diminishes at larger distances, and for this reason the analytical model is probably most accurate at comparatively large distances in the rock. The analytical solution does demonstrate general trends in the glass cooling rate, however. The cooling rate is faster for thinner glass sections or for higher rock thermal diffusivities.

The calculations for basalt were based on the same glass thickness as the calculations for tuff. The glass liner produced by an extruding penetrator operating in basalt would ordinarily be much thinner. As a result, the cooling rate would be greater than the rates suggested by the curves in Fig. 9.

2. Comparison With Experimental Data. Experimental values for the temperature at the inside diameter of the glass liner are available from thermocouple data from a laboratory test of a 75-mm-diam consolidating penetrator.[13] The test was conducted in dried tuff on June 20, 1973. Figure 10 compares the experimental data with cooling curves computed by the finite-element code. The time = 0 axis for the curves was chosen so that the initial temperatures coincide. The average penetration rate during this portion of the test was 0.085 mm/s.

The cooling curves in Fig. 10 illustrate the significance of the rock thermal conductivity. The near-coincidence of the calculated curve for $\lambda = 0.75$ W/m·K with the experimental data does not necessarily imply that the higher value of conductivity is correct. Differences from the experimental temperatures may also be due to other factors, such as possibly inaccurate representations of the penetrator temperature distribution or of the convection/radiation boundary condition. The fact that physical and thermal properties of individual rocks may vary significantly implies that calculations for a particular set of properties may only illustrate general trends, which can be applied to an entire class of rock, rather than accurate results.

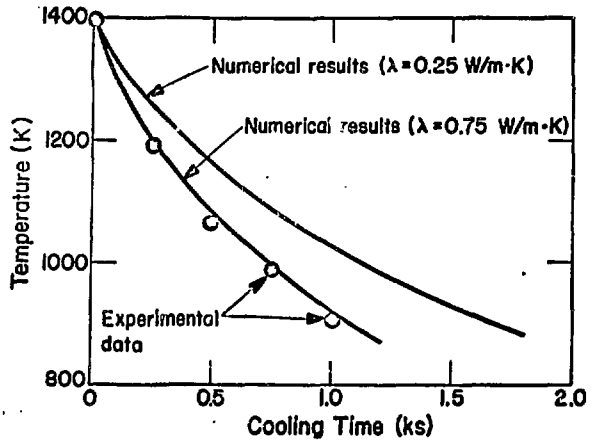

Fig. 10. Comparison of experimental temperature data with results from computer analyses; 75-mm penetrator in tuff.

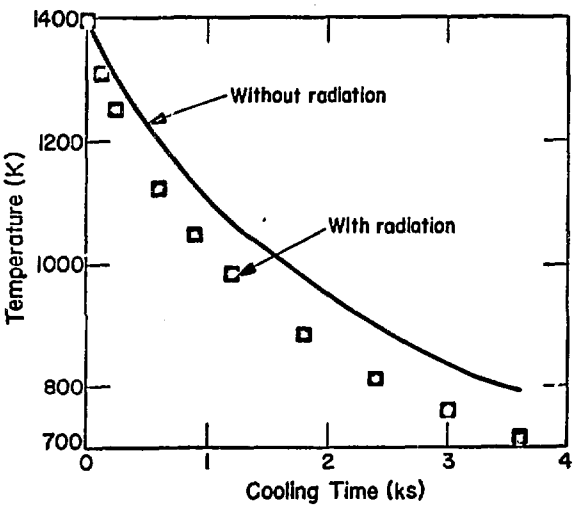

Fig. 11. Effect of radiation boundary condition on calculated cooling curves.

3. Effect of the Radiation Boundary Condition.

The effect of including the approximate radiation boundary condition is shown in Fig. 11. The one-dimensional transient computer model with λ = 0.25 W/m·K was used in the calculations. The importance of cooling by radiation is clear. The local effective radiation heat-transfer coefficient as defined in the appendix is of the same order of magnitude (10 to 100 $W/m^2 \cdot K$) as the convective heat-transfer coefficient.

B. Temperature Distributions and Glass Quality

As indicated in the discussion on thermal treatment processes, the magnitude of residual stresses in the glass liner is dependent on the temperature distribution across the glass thickness in critical temperature ranges. Specifically, from Eq. (1), the stresses are proportional to temperature differences from the average temperature. Figures 12 through 14 plot the maximum temperature difference as a function of changes in temperature from the melting point. The curves are based on calculations from the one-dimensional transient model.

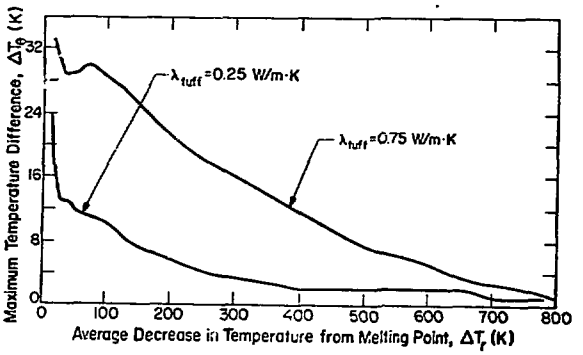

Fig. 12. Maximum difference from average glass temperature vs temperature change from the melting point; 50-mm penetrator in tuff.

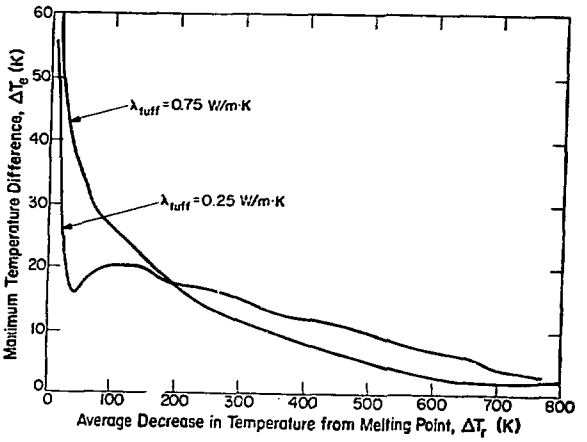

Fig. 13. Maximum difference from average glass temperature vs temperature change from the melting point; 75-mm penetrator in tuff.

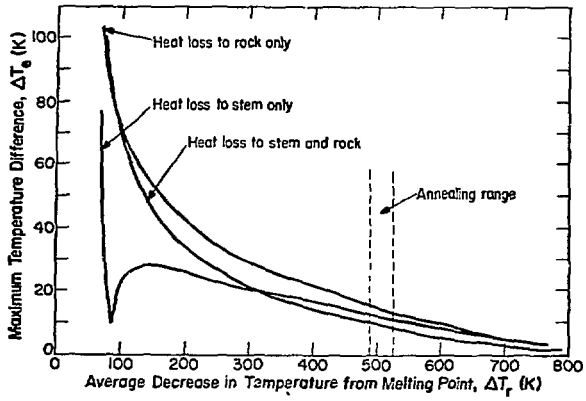

Fig. 14. Maximum difference from average glass temperature vs temperature change from the melting point; 75-mm penetrator in basalt.

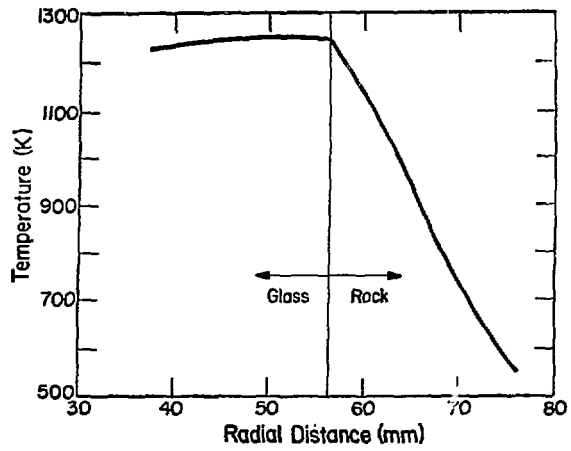

Fig. 15. Calculated radial temperature distribution in the annealing range of tuff-glass; 75-mm consolidating penetrator.

Several important trends are indicated by the curves. A higher thermal diffusivity for the rock has the effect of increasing the glass cooling rate at the rock/glass interface, which causes higher radial temperature gradients, particularly in the early stages of cooling. A comparison of Figs. 12 and 13 indicates the effect of design differences between the 50- and 75-mm-diam consolidating penetrators. Initially, cooling the inside surface of the liner by convection and radiation appears to result in a more rapid reduction of radial temperature gradients. For a low rock thermal diffusivity the inside edge of the liner quickly becomes the coolest part of the glass. This effect results in glass temperature differences that are higher than those produced by conduction cooling into the stem. For higher rock diffusivities, the coolest part of the glass remains at the glass/rock interface and the maximum temperature differences are generally lower than in the case of cooling by conduction.

For a 75-mm-diam penetrator operating in basalt, Fig. 14 shows curves for cases where all heat removed from the glass is restricted either to conduction into the rock or to convection and radiation at the inside surface of the glass. As in the case of low-conductivity tuff, restricting the heat losses to the coolant flow and stem results in a lower temperature at the inside surface of the liner. The curve exhibits an increase in the maximum temperature difference following the initially rapid decrease in this quantity. Restricting heat losses from the glass to conduction into the rock causes consistently higher temperature gradients than when the glass is cooled from both sides. This result, coupled with the observations about the effects of the thermal diffusivity of the rock, suggests that some balance should be maintained between conduction into the rock and the cooling on the inside liner surface. For rock with a comparatively high thermal diffusivity, a higher coolant flow rate seems appropriate.

The annealing range for basalt glass is indicated in Fig. 14. As mentioned earlier, precise viscosity-vs-temperature data for the more viscous tuff melt are not available. The annealing range for tuff glass is probably near ΔT_r = 100 or 200 K, corresponding to temperatures between 1200 and 1300 K.

For the 75-mm-diam penetrator in tuff, a typical value of ΔT_e in the assumed annealing range is 20 K. A calculated radial temperature distribution for temperatures in the annealing range is shown in Fig. 15. The calculations are for a thermal conductivity of 0.25 W/m·K. The cooling time is 300 s, which corresponds to a distance of 45 mm from the afterbody for a penetration rate of 0.15 mm/s.

Using 20 K for ΔT_e and assuming a Young's modulus of 6.9 x 10^{10} N/m^2 (~ 10^7 psi) and a Poisson's ratio of 0.22, Eq. (1) may be used to predict the magnitude of the residual stresses in the glass. The coefficient of thermal expansion in the annealing range of glasses is usually two to three times

the value measured for lower temperatures.[5] An experimental value of 6.9×10^{-6} K^{-1} was determined by Corning Glass Works for basalt glass in the temperature range 273 to 573 K.[7] For a coefficient of expansion of 1.4×10^{-5} K^{-1}, the stress calculated from Eq. (1) is 2.5×10^{7} N/m^2 (~ 3600 psi). For the 50-mm-diam penetrator in low-conductivity tuff, the stresses calculated from Eq. (1) are less than half this value. For basalt glass, still lower stresses are likely because the calculated radial temperature gradients were probably exaggerated by the assumed thickness of the glass.

These stresses are several times higher than those ordinarily permitted in commercial glasses.[14] Acceptable stress levels for commercial glass are usually established on the basis of the birefringence produced by the stresses. Because optical quality is not a consideration in the Subterrene glass liner, higher residual stress should be acceptable.

V. CONCLUSIONS

- Radial temperature distributions as a function of time or axial position can be predicted for Subterrene glass on the basis of one- and two-dimensional numerical models.
- Based on viscosity-vs-temperature data, a thermal treatment schedule can be devised to improve the quality of the glass liners.
- Residual stresses on the order of 10 MN/m^2 are estimated for glass liners produced by laboratory penetrator designs.
- Desirable cooling rates on the inside of the liner seem related to the thermal diffusivity of the rock. Higher cooling rates are possible for higher-diffusivity rock.
- An annular air space between the glass and the penetrator stem allows greater flexibility in varying the glass cooling rate.

APPENDIX

RADIATION BOUNDARY CONDITION

For the 75-mm-diam Subterrene penetrator, the surface at the inside diameter of the glass liner is cooled by convection to the coolant gas and by thermal radiation to the cooler stem. A precise formulation of the radiation part of the boundary condition would result in an integral equation involving configuration factors between differential elements. If the surfaces are non-diffuse or non-gray, additional complications arise.

A greatly simplified model was used to approximate the radiation boundary condition. Consider two infinite diffuse-gray concentric cylinders as shown in Fig. A-1. The inside cylinder is assumed to be at a uniform temperature T_1 and the outside cylinder is at a uniform temperature T_2. The net thermal radiation energy exchange between the cylinders is[15]

$$Q_2 = \frac{A_2 \sigma (T_2^4 - T_1^4)}{\frac{r_2}{r_1}\left(\frac{1}{\epsilon_1}\right) + \frac{1}{\epsilon_2} - 1} \qquad \text{(A-1)}$$

where subscripts 1 and 2 refer to the inside and outside cylinders, and

Q_2 = net thermal radiation leaving the outside cylinder,

A_2 = radiating surface area of the outside cylinder,

σ = Stefan-Boltzmann constant,

ϵ = emissivity of thermal radiation.

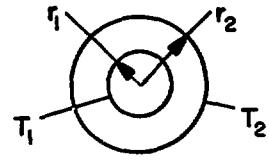

Fig. A-1. Diffuse-gray cylinders of infinite length.

The radiation boundary condition may be expressed in terms of an effective heat-transfer coefficient between the glass-liner temperature T_2

and the bulk temperature of the coolant flow, T_c.[16] This coefficient is defined by equating the net radiation energy in Eq. (A-1) to the effective convection heat transfer.

$$Q_2 = \frac{A_2\sigma\,(T_2^4 - T_1^4}{\frac{r_2}{r_1}\left(\frac{1}{\varepsilon_1}\right) + \frac{1}{\varepsilon_2} - 1} = A_2 h_{eff}\,(T_2 - T_c). \quad \text{(A-2)}$$

The resulting expression for the heat-transfer coefficient is

$$h_{eff} = \frac{\sigma\,(T_2^4 - T_1^4)}{\frac{r_2}{r_1}\left(\frac{1}{\varepsilon_1}\right) + \frac{1}{\varepsilon_2} - 1} \frac{1}{T_2 - T_c}. \quad \text{(A-3)}$$

The total heat transfer to the coolant and stem from the inside surface of the glass liner may now be expressed in terms of coolant temperature and total heat-transfer coefficient,

$$h_{total} = h_{eff} + h_c, \quad \text{(A-4)}$$

where h_c is the convection heat-transfer coefficient.

The problem of determining appropriate "uniform" temperatures T_1 and T_2 remains. One approach could be to assume some typical values. Alternatively, a means could be devised to try to accommodate the fact that, as the axial distance increases, the magnitudes of the local temperatures decrease and consequently the thermal radiation flux decreases. This method requires the iterative determination of local coefficients at nodal points along the glass boundary. Expression (A-1) for radiation-energy exchange is no longer accurate because of the nonuniformity of temperatures; however, its use is somewhat justified by the fact that particular axial locations in the glass liner will exchange energy mostly with a small region of the stem directly opposite.

The temperature distribution along the stem may be estimated by considering an infinite hollow cylinder with convection at the inside and outside surfaces, Fig. A-2. If one end is maintained at the constant temperature T_b, the axial temperature distribution is[17]

$$\frac{T(x) - T_c}{T_b - T_c} = \exp\left(-x\sqrt{\frac{hP}{\lambda A}}\right) \quad \text{(A-5)}$$

where

T_c = ambient or bulk temperature of the coolant fluid,

h = convection heat-transfer coefficient,

P = perimeter in contact with the coolant fluid,

λ = thermal conductivity of the cylinder,

A = conducting area of the cylinder.

The heat-transfer coefficient and fluid temperature are assumed to be the same on the inside and outside of the cylinder. Radiation energy exchange is neglected.

For a one-dimensional transient model of heat-transfer processes in Subterrene glass, Eq. (A-5) is replaced by

$$\frac{T(x) - T_c}{T_b - T_c} = \exp\left(-Vt\sqrt{\frac{hP}{\lambda A}}\right) \quad \text{(A-6)}$$

where t is time and V is the penetration rate.

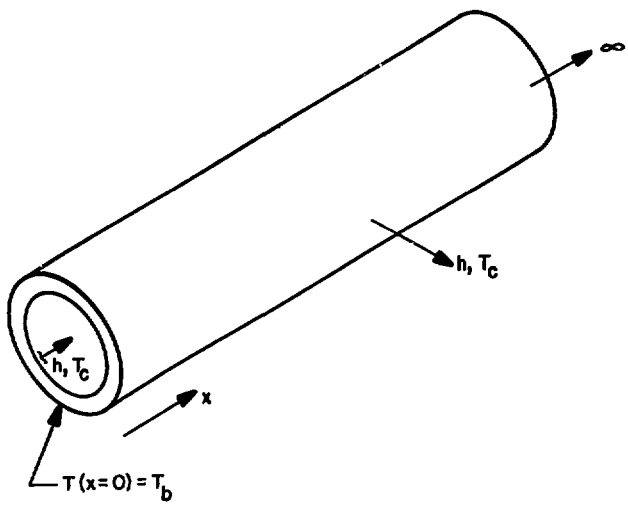

Fig. A-2. Infinite hollow cylinder for estimating the axial temperature distribution along the molybdenum stem.

Equations (A-5) and (A-6) were used in conjunction with Eq. (A-3) to estimate thermal radiation effects at the inside boundary of the glass. Thermal emittances of 0.2 for the stem and 0.8 for the glass were used, with a coolant temperature of 500 K and a stem base temperature, T_b, of 1000 K.

REFERENCES

1. J. W. Neudecker, "Design Description of Melting-Consolidating Prototype Subterrene Penetrators," Los Alamos Scientific Laboratory Report LA-5212-MS (February 1973).

2. J. W. Neudecker et al., "Design and Development of Prototype Universal Extruding Subterrene Penetrators," Los Alamos Scientific Laboratory Report LA-5205-MS (March 1973).

3. M. C. Krupka, "Phenomena Associated with the Process of Rock Melting, Application to the Subterrene System," Los Alamos Scientific Laboratory Report LA-5208-MS (February 1973).

4. W. Giegerich and W. Trier, Eds., Glass Machines (Springer Verlag, Inc., New York 1969), p. 18.

5. E. B. Shand, Glass Engineering Handbook (McGraw-Hill, Inc., New York, 1958), pp. 103-118.

6. J. R. Hutchins III, and R. V. Harrington, "Glass," in Encyclopedia of Chemical Technology (John Wiley and Sons, Inc., New York), pp. 533-604.

7. J. C. Rowley, Los Alamos Scientific Laboratory, unpublished technical memorandum (1972).

8. H. S. Carslaw and J. C. Jaeger, Conduction of Heat in Solids (Oxford University Press, London, 1959), p. 54.

9. R. G. Gido, "Internal Temperature Distribution of a Subterrene Rock-Melting Penetrator," Los Alamos Scientific Laboratory Report LA-5135-MS (January 1973).

10. J. C. Jaeger, "Cooling and Solidification of Igneous Rocks," in Basalts, H. H. Hess and A. Poldervaart, Eds., (John Wiley and Sons, Inc., New York 1968), pp. 503-536.

11. R. G. Lawton, "The Ayer Heat Conduction Computer Program," Los Alamos Scientific Laboratory report in preparation.

12. D. J. Murphy and R. G. Gido, "Heat Loss Calculations for Small Diameter Subterrene Penetrators," Los Alamos Scientific Laboratory Report LA-5207-MS (February 1973).

13. G. E. Cort, "Test Data for 75-mm-diam-Consolidator - Part II," Los Alamos Scientific Laboratory, to be published.

14. G. W. Morey, The Properties of Glass (Reinhold Publishing Corp., New York, 1954), p. 167.

15. R. Siegel and J. R. Howell, Thermal Radiation Heat Transfer (McGraw-Hill, Inc. New York, 1972), p. 226.

16. R. G. Gido, "Internal Temperature Distribution of a Subterrene Rock-Melting Penetrator," Los Alamos Scientific Laboratory Report LA-5135-MS (January 1973).

17. V. S. Arpaci, Conduction Heat Transfer (Addison-Wesley Co., Reading, Massachusetts, 1966), p. 147.